Geological Quarterly, 2023, 67: 58
DOI: http://dx.doi.org/10.7306/gq.1735

This paper is a part of *Climate and environmental changes recorded in loess covers* (eds. Maria Łanczont, Przemysław Mroczek and Wojciech Granoszewski)

Electrical resistivity tomography as a modern tool for identifying loess covers – case study the Magdalenian site Wilczyce 10 (Sandomierz Upland, Poland)

Bogdan ŻOGAŁA[1], Przemysław MROCZEK[2, *], Maria ŁANCZONT[2] and Iwona STAN-KŁECZEK[1]

[1] University of Silesia, Institute of Earth Sciences, Faculty of Natural Sciences, ul. Będzińska 60, 41-200 Sosnowiec, Poland, ORCID: 0000-0002-6397-5599 [B.Ż.], 0000-0003-0757-5926 [I.S.-K.]

[2] Maria Curie-Skłodowska University, Institute of Earth and Environmental Sciences, al. Kraśnicka 2d, 20-718 Lublin, Poland ORCID: 0000-0003-2702-5577 [P.M.], 0000-0002-0459-8658 [M.Ł.]

Żogała, B., Mroczek, P., Łanczont, M., Stan-Kłeczek, I., 2024. Electrical resistivity tomography as a modern tool for identifying loess covers – case study the Magdalenian site Wilczyce 10 (Sandomierz Upland, Poland). Geological Quarterly, 67: 57; https://doi.org/10.7306/gq.1735

This research utilises electrical resistivity tomography (ERT) in geophysical surveys conducted in the vicinity of a Magdalenian (Upper Palaeolithic) site in Wilczyce, Poland, focusing on loess covers and their litho- and pedological formation in relation to bedrock. The study yields several key findings: ERT effectively determines the depth of the rock mass. Measurements were made along two 200 m long measurement lines. High-resolution ERT sequences enable precise boundary delineation between layers, uncovering distinct palaeorelief and identifying large palaeo-cavities. Achieving reliable results requires well-designed research plans and the use of the Schlumberger-Wenner or gradient array. The study also confirms the continuity of the L1 loess cover, variable thickness (ranging from 5 to 15 metres), and lithological identification through electrical resistivity imaging. The presence of a wavy palaeosurface beneath the loess layer indicates past landscape undulations, offering insights into geomorphological evolution and soil transformations in the presence of the loess mantle. While interglacial palaeosol (S1) was reliably detected, identifying lower-ranked mid-loess palaeosols posed challenges, highlighting complexities in soil formation processes and limitations in discerning underdeveloped horizons with electrical resistivity cross-section. The study specifically examines the sequence of loess-palaeosol S0-L1-S1, providing valuable insights into the geological and palaeoenvironmental context of the Late Magdalenian site.

Key words: Weichselian, Palaeolithic, palaeorelief, palaeosol, interpretation, Schlumberger-Wenner array.

INTRODUCTION

In palaeoenvironmental research, particularly in the recognition of loess layers and archaeological sites commonly found within them, the 2D resistivity method, known as electrical resistivity tomography (ERT) or electrical resistivity imaging (ERI), plays a crucial role. Its primary advantages lie in its non-invasive nature and ability to quickly conduct tests and generate results. ERT/RI helps address various challenges, including determining the extent, thickness, and depth of loess layers, reconstructing palaeorelief, identifying fossil soils, and locating Palaeolithic sites inhabited by early humans (Łanczont et al., 2014, 2015a, b, c; Żogała, 2015; Ling et al., 2016; Zeng et al., 2016). It enables the resolution of several issues, including the determination of the extent, thickness, and depth of loess layers, the reconstruction of palaeorelief, the separation of fossil soils, and the location and identification of archaeological sites inhabited by Palaeolithic people. The reconstruction of palaeorelief holds significant importance in archaeology, especially when the original arrangement of cultural layers has been disrupted due to post-depositional processes, primarily periglacial processes (Deeben et al., 2010), which frequently occur in areas particularly susceptible to slope processes. Cultural artifacts carried by solifluction-deluvial flows may have been displaced over varying distances. Hence, questions arise regarding their original placement and the necessity of reconstructing the former topographical surface from the settlement period. Research conducted using this method often serves as preliminary research, helping to delineate potential excavation sites. In the field of hydrogeophysics, which has seen recent intensive development, the ERT method ranks among the most crucial geophysical methods. Its high sensitivity characterises the hydromechanical and structural properties of loess, which are pivotal for understanding its stability as both soil and subsurface structure (Qin et al., 2020). It is also used to identify water infiltration that can initiate mass movement (Zhao et al., 2020; Feng et al., 2020; Zhang et al., 2022; Bian et al., 2022) and for detecting reservoir waters with significant spatial heterogeneity

* Corresponding author, e-mail: przemyslaw.mroczek@mail.umcs.pl

Received: December 21, 2023; accepted: February 28, 2024; first published online: March 13, 2024

(Palis et al., 2017; Whiteley et al., 2019). The presented research aimed to explicitly recognise the loess cover and the palaeorelief at the archaeological site of Wilczyce 10 near Sandomierz, Poland, using the electrical resistivity tomography method.

FACTORS DETERMINING THE ELECTRICAL RESISTIVITY OF ROCKS

The resistivity method is based on resistivity changes in the geological medium. Changes in resistivity result from both natural factors like the structure and texture of the rocks (Plewa and Plewa, 1992; Schön, 1996; Żogała and Stan-Kłeczek, 2022) and artificial: as a result of human activity, e.g., mining, drilling, earthworks, or contamination (Ryncarz, 1993; Mendecki et al., 2013; Żogała, 2013). Mass movement is also important (de Bari et al., 2011; Fabregat et al., 2017). Each type of rock has a specific range of resistivity values. The resistivity range for a specific type of rock can vary widely (Table 1).

The wide range of resistivity values depends on several factors: water content and mineralisation degree (the higher the mineralisation, the lower the electrical resistivity), stratification, and clay minerals. A specific parameter affecting the resistivity is the porosity of the rocks. In the case of dry pores, the resistivity value increases significantly; conversely, when the rocks are saturated with water, it decreases markedly. Clay minerals, being excellent conductors, strongly reduce the resistivity of the rocks in which they are present. The water content is another factor that lowers the resistivity value; the more mineralised the water, the lower the resistivity. These factors illustrate that without knowledge of the lithology. It can only infer changes in an electrical parameter, namely the separate resistivity layers.

PARAMETERS AFFECTING THE RESISTIVITY VALUES OF LOESS SEDIMENTS

Loess deposits are unique sediments for resistivity measurement, primarily due to their aeolian accumulation. Due to the physical and chemical similarities among various loess layers, they relatively often form covers composed of strata from different periods, but exhibiting no lithological differences. Accurate measurement of the loess covers' thickness is feasible only when the underlying layer exhibits a distinct resistivity contrast. From the perspective of recognising loess layers, their wide resistivity range is crucial (Table 1). This range mainly results from lithological diversity, including sandiness, the presence of clay minerals and soil sediments, and, to a lesser extent, their porosity and water content.

Polish periglacial loess typically comprises quartz (60–80%), aluminosilicates (10–20%), iron oxides (several percent), and calcium carbonate (up to 15%; Skurzyński et al., 2019, 2024; Skurzyński, 2020). Minor quantities of micas, glauconite, phosphate rock, and heavy minerals are also present (Malinowski, 1971; Racinowski, 1976; Chlebowski and Lindner, 1991; Łanczont and Wilgat, 1994; Maruszczak and Wilgat, 1995). The clay minerals mainly include kaolinite and hydromicas. Their presence varies across different loess horizons. In the upper part of the younger loess (L1), the content ranges from 1–3%, while in older horizons, it can reach up to 15% (Malinowski, 1959; Kowalska et al., 2022).

An increase in clay minerals significantly reduces electrical resistivity. Effective recognition of loess sequences is possible when different loess fractions vary in clay mineral content. However, within a given loess facies, the concentration of these minerals should remain relatively consistent (Żogała et al., 2015).

Soil materials, which are slightly different from loess, become less effective electrical conductors due to changes in the granulometric and mineralogical composition of the loess material due to the soil-forming process. A decrease in resistivity in soil sediments is observed when they mix with loess material, for instance, due to solifluction or when loess separates soil layers. Consequently, the lower resistivity values recorded by measuring equipment reflect the entire geological rock complex (Żogała et al., 2015). Iron oxides also lower the electrical resistivity value. Loess composition is predominantly dust fraction, constituting 60–70%, followed by up to ~20% each of the clay and sand fractions (cf. Łanczont et al., 2014, 2015b). The average loess fraction size is 0.02–0.05 mm. Colluvial and alluvial loess contains more sand fractions, while weathered (clay) loess has a higher clay fraction. Generally, smaller fractions correspond to lower resistivity values.

Porosity and moisture content also significantly impact the measured electrical resistivity. These two factors are interrelated. Loess porosity is high, reaching approximately 40-60% (Frankowski and Grabowski, 2006), and tends to decrease with depth. A reduction in porosity always accompanies a decrease in resistivity. Conversely, lower moisture content results in increased resistivity.

Table 1

The electrical resistivity ranges for rocks characteristic of loess areas

Type of rocks	Resistivity [m]	References
Limestone	50–5000	Loke (2011)
Clay	1–100	
Shale	20–2000	
Gravel	100–10000	Ward (1990)
Loess	30–100	Knödel et al. (2007)
Mules	20–50	
Gravel and sand	50–10000	
Clay (wet)	5–30	
Clay (dry)	>1000	
Sand above the groundwater table	250–10000	Stenzel and Szymanko (1973)
Waterlogged sands, gravels	80–350	
Loess	20–60	
Silt, clay	35–80	
Loess	30–100	Łanczont et al. (2015b)

Loess deposits are characterised as poorly diagenetic rocks. In this context, bound water is crucial rather than free water in the pore space. The degree of water mineralisation significantly affects electrical resistivity; higher mineralisation always leads to lower resistivity. Similarly, a reduction in moisture content corresponds to an increase in resistivity.

METHODS

Geophysical research, which constitutes the main subject presented in this article, was complemented by analyses of the litho- and pedological formation of loess covers, based on a profile from drilling carried out at the culmination of a loess hill (Łanczont et al., 2014, 2015b). Analyses of grain size, humus content, and carbonates were conducted on the material obtained. The drilling reached the lower boundary of the Vistulian (Weichselian) loess (L1 = MIS2–MIS4), ending at the upper horizons of the Last Interglacial palaeosol complex (S1 = MIS5). Each sample studied represents a 10 cm interval. Particle size measurements in the range of 0.01–2000 μm were performed using a *Malvern Mastersizer 2000 HydroG* diffractometer. The results obtained were used to calculate the percentage share of three basic fractions – clay (<5.5 μm), silt (5.5–63 μm), and sand (>63 μm). Additionally, grain size indicators such as mean grain, kurtosis, and skewness were calculated according to Folk and Ward (1957), as well as grain size index (GSI 21-52/<21 μm) and U-ratio (16-44/5.5-16 μm) indicators (cf. Ujvari et al., 2016). To visualise the grain size distribution in individual samples, a heat map was developed with particle size measurements divided into 100 logarithmic intervals. The humus content was determined using the Scheibler method, and Fe_2O_3 – using a colorimetric method.

CHARACTERISTICS OF THE STUDY AREA

LOCATION, GEOLOGY AND RELIEF

Geophysical studies were conducted around the Late Magdalenian site of Wilczyce 10 (Fiedorczuk and Schild, 2002; Schild, 2014; Łanczont et al., 2014, 2015b), located in the Opatów Upland, on the eastern foreland of the Świętokrzyskie Mountains (Gilewska, 1972). This is the northeastern part of the Sandomierz loess patch, which forms the central part of the Polish section (Fig. 1A) of the North European Loess Belt (e.g., Haase et al., 2007; Li et al., 2020; Lehmkuhl et al., 2021).

The study area is located in the contact zone of the Opatów Anticlinorium, which is the eastern extension of the Łysogóry Anticlinorium zone and the Northern Syncline. Its structural plan was ultimately shaped during the Hercynian orogeny (Samsonowicz, 1960; Bielecka, 1968b; Tomczyk, 1974), and superimposed on it is a Middle Miocene zone of depressions, likely tectonic, which also includes the Opatówka region. This is associated with the development of the northern Fore-Carpathian Depression (Bielecka, 1968b). The Opatówka tectonic depression is filled with Middle Miocene sediments, when this region was incorporated into the area of the fore-mountain basins repeatedly occupied by the oscillating sea bays. These are sands and silts with inserts of carbonaceous clays and brown coals, covered by a discontinuous series of glauconitic sands, as well as limestones and marls interspersed with shell limestones (Bielecka, 1968a). The Quaternary is represented by two complexes of glacigenic sediments, separated by an interglacial river series. The older complex, from the South Polish glaciation, is formed as a till clay underlain by a series of glaciofluvial sands. The younger Middle Polish glacial period is also documented by tills, glaciofluvial series, as well as submoraine and supramoraine varved clays and silts, and patches of submoraine loess (Czarnecki, 2005). The youngest link in the Pleistocene sediments is formed by a loess cover up to 25 m thick in culmination zones (Makowski, 1976). The continuous loess mantle covers older landforms.

In the landscape of the Opatów Upland in the Wilczyce area, the central position is occupied by the east-west oriented valley of the Opatówka River, consisting of several distinct basin-like expansions and narrow structural sills (Fig. 1B). The depth of its contemporary incision is ~40 m. North of the Opatówka River valley, the maximum heights of the plateau reach 210–217 m a.s.l., while to the south, they exceed 230 m a.s.l. (Fig. 1B, C). The northern slopes of the valley are noticeably longer and gentler than the southern ones, and they also have an uneven course, which is conditioned by the presence of plateau outcrops in the form of promontory peninsulas – loess remnants representing the full range of terrain exposure. The loess plateau has a wavy or flat surface, encompassing three hypsometric levels (Fig. 1B). The plateau is divided by a system of dry erosional-denudational valleys, with different development to the north and south of the Opatówka River valley. They form highly branched systems. The largest of them is located near Wilczyce.

LOESS COVER IN THE AREA OF WILCZYCE 10 SITE AND ITS STRATIGRAPHIC DIFFERENTIATION

The archaeological site Wilczyce 10 is situated in the culmination zone of a remnant loess promontory at an elevation of 195–197.4 m a.s.l., and 37.4 m above the bottom of the Opatówka valley (Fig. 1B, C; Bałaga et al., 2008; Łanczont et al., 2014, 2015b). This hill forms the eastern part of a segmented loess ridge, separating two basin-like expansions of the valley. The culmination of the promontory with the site is almost flat, but the slopes are quite steep, especially from the W, NW, and NE sides. The slope system is divided by a series of side hollows and small basin-like valleys. The largest of these, bordering the west of the described culmination and perpendicular to the Opatówka river valley, is 600 m long (Fig. 1C). The top part of the loess is cut by a network of polygonal structures (Łanczont et al., 2014, 2015b).

The loess cover surrounding the Wilczyce 10 site is formed by the youngest loesses of the most recent cycle of aeolian dust accumulation during the last glaciation. They are designated as LM loess according to Maruszczak (1991), the main part of which consists of younger upper loess (LMg), lying on younger middle and lower loesses (LMs, LMd) separated by soil horizons of lower stratigraphic rank, among which a fossil gley/cambic soil correlated with MIS 3 (gi/LMd) is distinguished. The Vistulian loesses rest on the top of the soil complex from the Last Interglacial s.l. (=MIS 5) and are formed on older upper loess (LSg; MIS 6). Additionally, at the top of the LMg loess, a contemporary soil (GH) forms, which is more accurately described as a Late Glacial-Holocene soil corresponding to MIS 1 (e.g., Maruszczak 1991; Mroczek, 2018). According to the stratigraphy by Kukla and An (1989) as modified by Marković et al. (2008, 2015), this sequence is recorded as: S0-L1LL1-L1SS1-L1LL2-S1-L2LL1.

Based on field investigations (archaeological excavations, soil mapping) and the results of laboratory analyses of the drill core, it can be observed that the loess cover in the vicinity of the site display variation in terms of structure, lithology, physicochemical properties, and age (Łanczont et al., 2014, 2015b). The boundaries between the individual layers clearly denote horizons of buried soils of different stratigraphic ranks and erosional surfaces (Fig. 2).

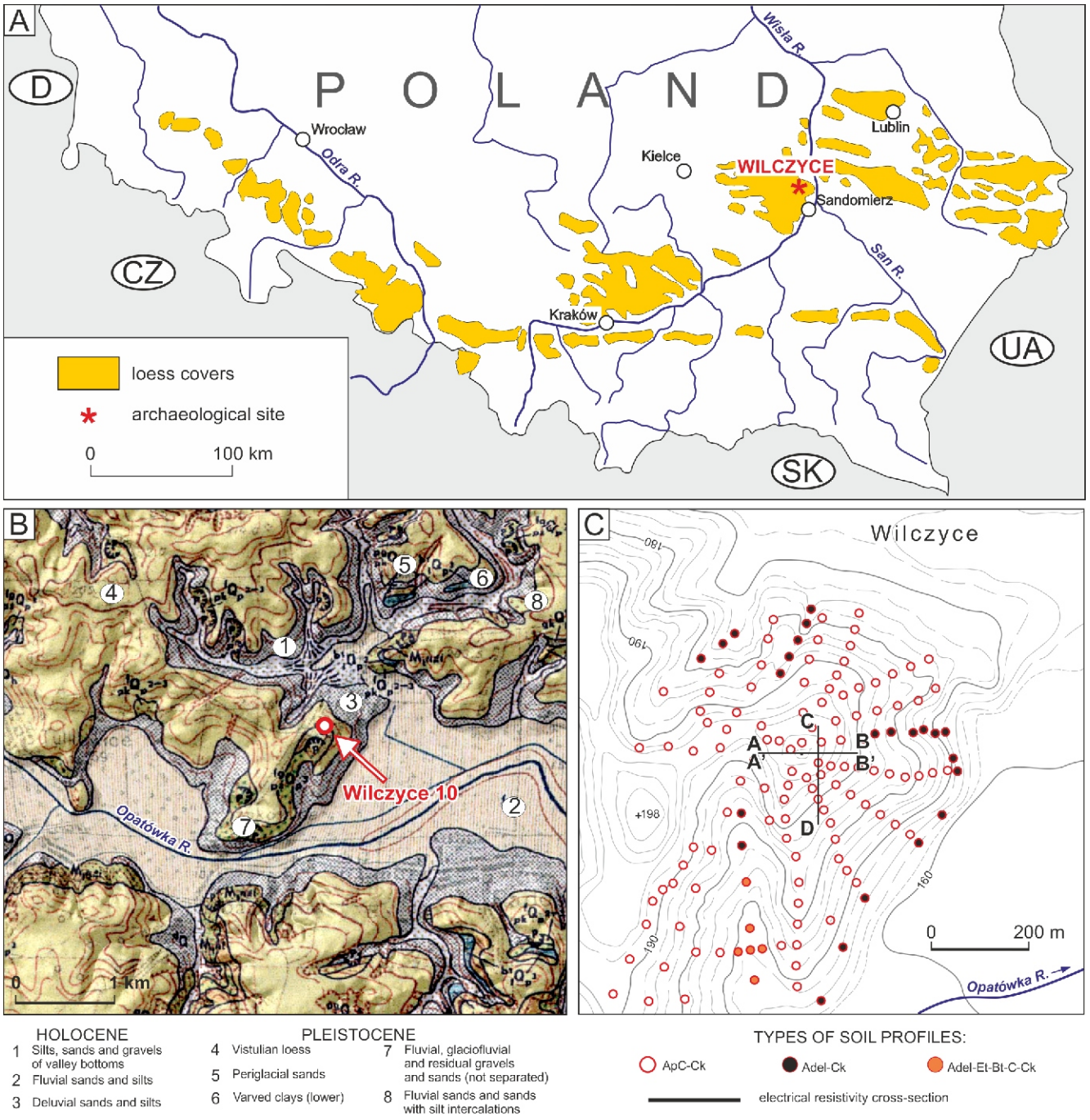

Fig. 1. Location of the study area depicted against: (A) the extent of loess covers in Poland as identified by Maruszczak (2001); (B) surface sediments mapped by Bielecka (1968a, b); and (C) a hypsometric map showing the distribution of electrical resistivity profiles (A–B, A'–B' and C–D) and soil probes, as modified from Łanczont et al. (2014)

In the entire analysed sequence, the dominant fraction is silt, constituting on average 83.5% of the total mass (Fig. 3A, B). Its share varies widely from 45.4 to 87.9%. The average content of the clay fraction was 8.2%, with extreme values of 5.8 and 10.8%. Characteristic percentages for the sand fraction are as follows: 8.1% and a range between 3.1% and 38.5%. In the heatmap image (Fig. 3B), it is clear that the dominant subfractions are medium and coarse silt (mSi and cSi). Additionally, there is an enrichment in clay in soil horizons, while in the sand of the primary loess layers – but in this case, the increase in its share often is limited to individual samples (thin layers).

Generally, the grain size indices are not very variable, and their values change significantly at the boundaries of adjacent units reflecting the litho- and pedological formation. The mean grain size (median) ranges from 16.2 to 37.4 μm, with the overall sequence averaging 22.3 μm. The average standard deviation for the described sequence is 1.8, varying widely from 1.5 to 3.5. Based on this, the sediments should be considered as poorly and very poorly sorted, but generally, the sorting improves upwards. The average skewness for the entire analysed sequence is 0.3, changing from almost 0.0 to 0.4, thus from symmetrical to positively skewed. Meanwhile, the kurtosis value for the entire sequence varies widely from 0.6 (flat, broad curve) to 1.5 (sharp-peaked curve). The high variability of the GSI and U-ratio indicators suggests that loess formation took place in a highly dynamic environment. The curves characterising both aforementioned indices show similar trends, and noticeable step changes in their values are observed.

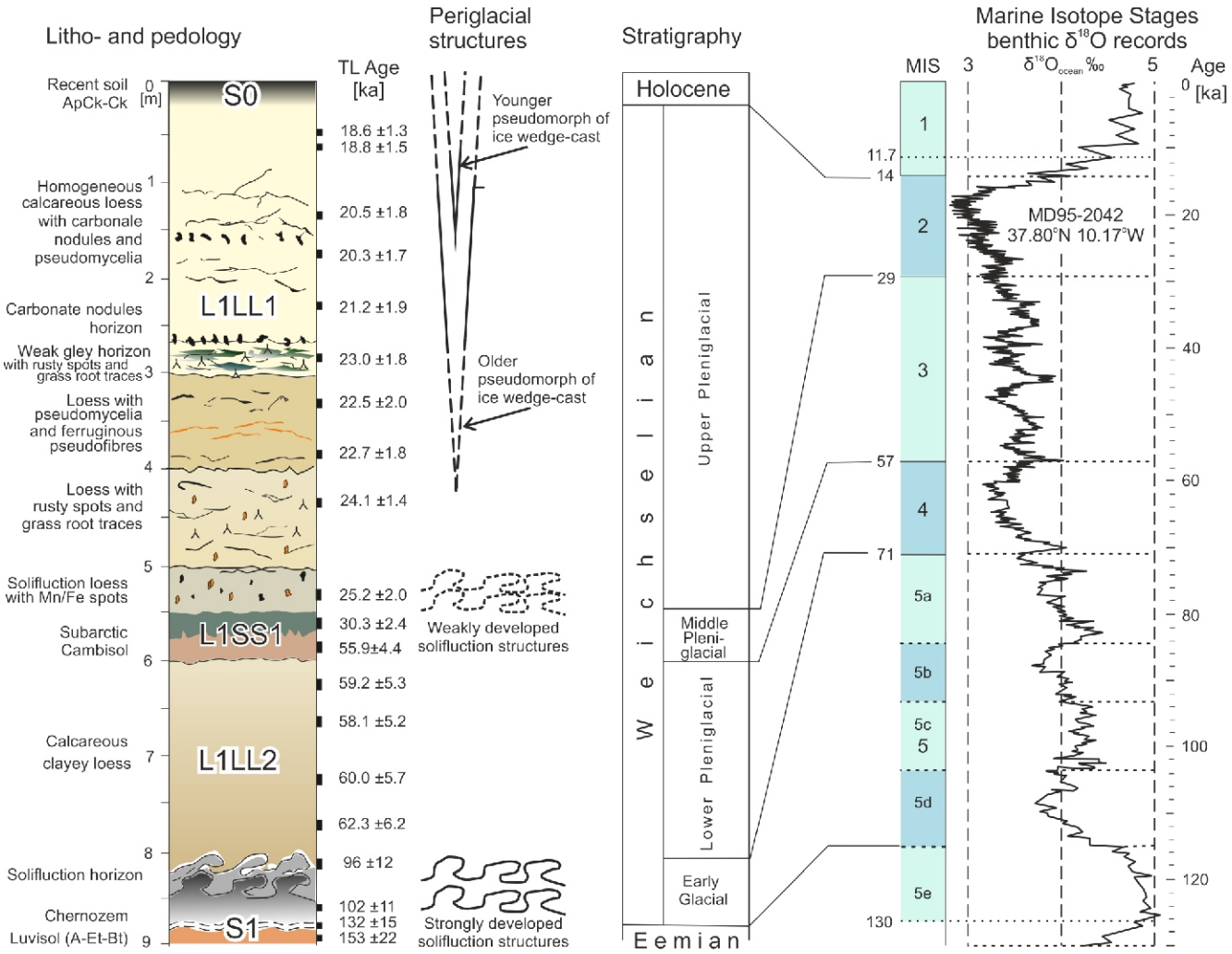

Fig. 2. Characterisation of loess-palaeosol sequences from a borehole drilled at the Wilczyce 10 archaeological site, together with dating results, stratigraphic interpretation and correlation with marine sediment isotope-oxygen stages (MIS) according to Łanczont et al. (2015b) with modifications

Explanations in the text

Almost the entire sequence is carbonaceous. The only layers devoid of $CaCO_3$ are the S1 palaeosol unit (drill core bottom) and the contemporary S0 soil profile (top). The top of the loess under the mid-loess palaeosol L1SS1 (correlated with MIS 3) is also carbonate-free, dividing the profile in terms of $CaCO_3$ richness into two parts: below, the sediments have a carbonate compactness of up to a maximum of 7%; whereas above, it ranges from 7 to 12%. Additionally, in the upper unit, their maximum values are recorded in the lower part of the gleyed loess with features of an initial horizon (at a depth of 4–5 m) and in the youngest top section under the contemporary soil (~1.5 m).

The humus content essentially reflects the degree of soil transformation of the loesses (Fig. 3A). Its maximum values (up to 1.6%) were found in the contemporary soil (S0) and the top of the loess L1LL1. In the other units of the profile, its content remains at ~0.2%. Only in the upper horizon of the interstadial soil L1SS1 and in the Early Glacial Chernozem soil is an increase in humus content (0.4–0.7%) noticeable.

Increased Fe_2O_3 content (2–3%) has also been documented within the palaeosol L1SS1 and the loesses underlaying it. In the remaining samples, the iron oxide content was low, at the level of 1.5–2%. Exceptionally low Fe_2O_3 content were found in the top horizon of the S1 palaeosol complex.

Soil cover mapping around the archaeological site (Łanczont et al., 2014, 2015b; Mroczek, 2018) demonstrated strong erosion of the Late Glacial-Holocene soil (S0) formed at the top of the loess L1LL1. This was confirmed by analyses of archaeological excavations and most soil probes (Fig. 1C), where the widespread occurrence of simple ApC-Ck soil profiles was documented, that is, soils formed contemporarily directly on the top of the carbonate loess. The original formation of soils in the Luvisols type is evidenced by well-developed profiles with a sequence of Adel-Et-Bt-C-Ck horizons, buried at the bottoms of slope hollows. The colluvial layer in their top is composed of redeposited older soil material.

The significant degree of erosion of the loess cover, interpreted based on the absence of natural soil cover (zonal soils of the Luvisols type), translates into the degree of preservation of cultural layers at the Late Magdalenian site (cf. Schild, 2014). The distribution of artifacts is closely related to the system of polygonal structures interpreted as pseudomorphs of ice wedges, with an OSL age corresponding to the late part of the Upper Pleniglacial (Kolstrup and Schild, 2014). Artifacts occur directly under the topsoil or at a depth of only a few tens of centimeters in the fill of a depression in the node of a polygonal network (Kolstrup and Schild, 2014).

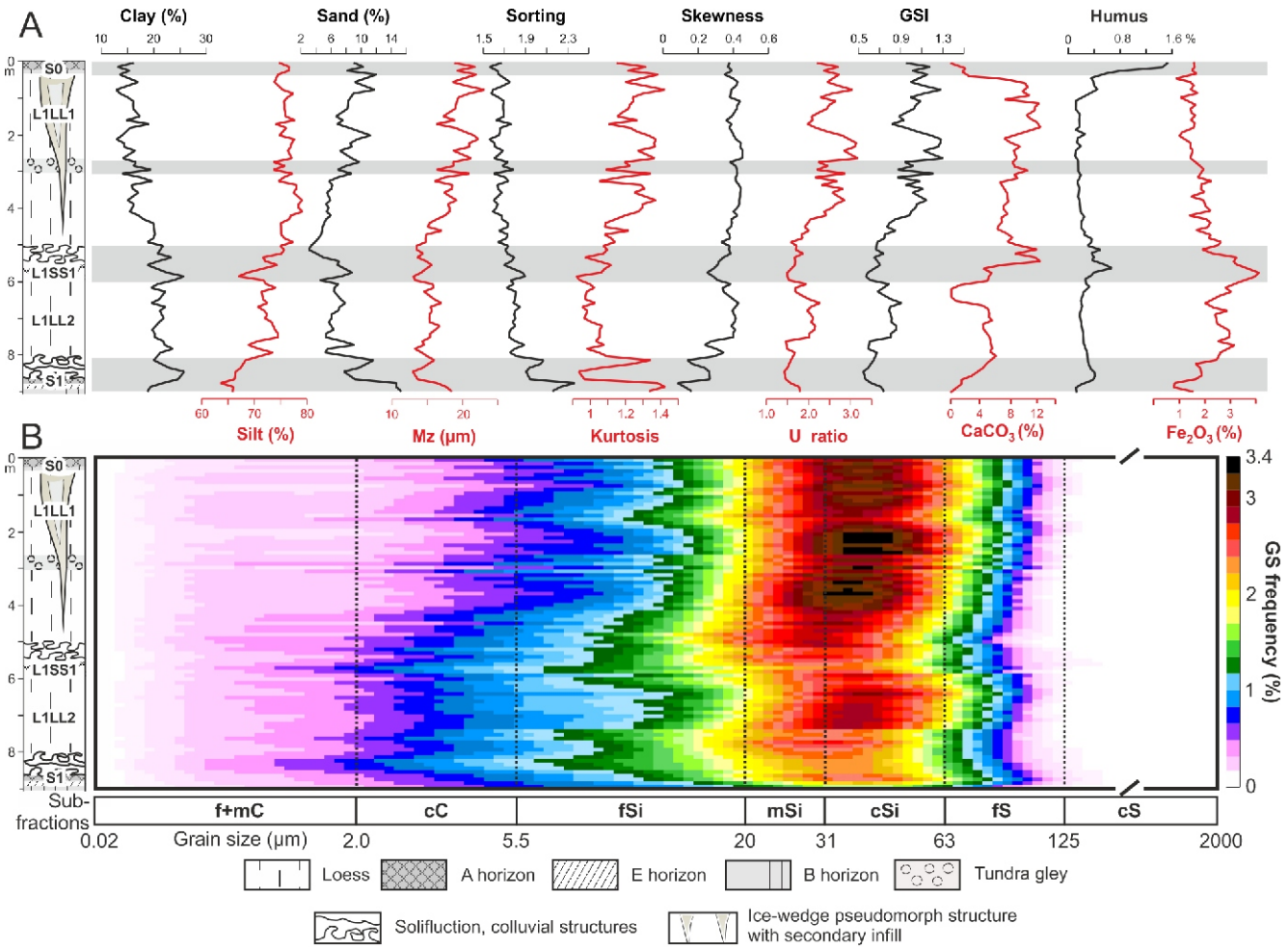

Fig. 3. Characteristics of the loess-palaeosol sequence in the drill core at the Wilczyce 10 site: A – main fractions, granulometric indices, humus, Fe_2O_3 and $CaCO_3$ content; B – heat map showing grain size (GS) frequency and subfractions C – clay, Si – silt, S – sand, f – fine, m – medium, c – coarse)

GEOPHYSICAL MEASUREMENT

BASICS OF RESEARCH METHODOLOGY

ERT is based on standard variants of resistivity surveys like vertical electrical sounding and electrical resistivity cross-section. The quantity directly measured in the field is the electrical resistance $R = V/I$, which is proportional to the apparent resistivity :

$$= kR \; [\;\; m]$$

where: k is the geometric factor which depends on the arrangement of selected arrays [m].

In the ERT method, resistivity measurements are carried out automatically in all sequences with a "momentary and stable" measuring array with a digital record in the meter's memory (Fig. 4).

The results obtained are interpreted using the *Res2Dinv* software. When measurements are made in morphologically diverse terrain, the inversion process accounts for the topography, including considering the stabilised electrodes' heights.

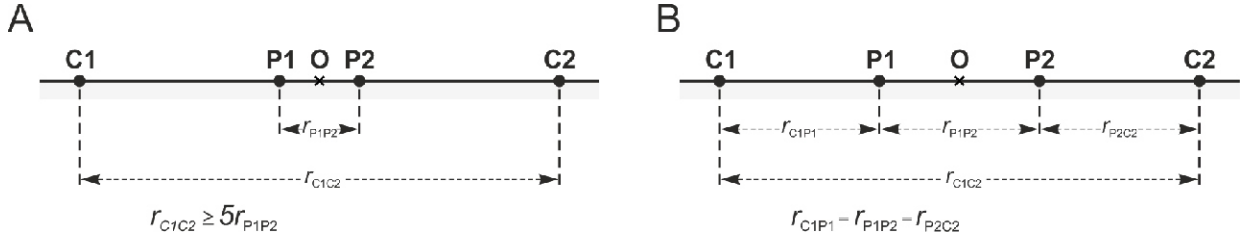

Fig. 4. Diagram of measurement array: Schlumberger (A) and Wenner (B)

O – a centre of the momentary measurement array (point to which the measured value of apparent resistivity refers; **Żogała, 2013**)

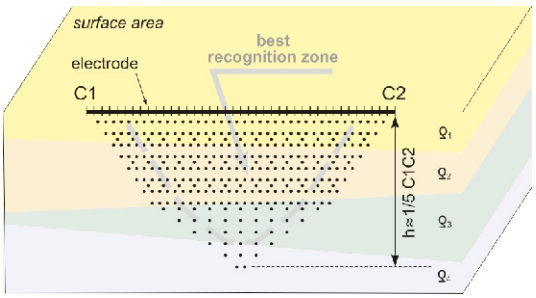

Fig. 5. Apparent resistivity measurement points distribution beneath sequence C1–C2 using the Schlumberger-Wenner array, with the grey line showing the best fit zone from the inversion process

The final outcome of this inversion is a resistivity cross-section along the studied profile, depicting variations as a function of depth.

Good results are achieved in recognising loess covers using the Schlumberger-Wenner measurement protocole, consisting of two Wenner and Schlumberger arrays. Figure 5 shows the distribution of apparent resistivity points under the measurement profile.

The method enables continuous detection of electrical layers at depths ranging from several metres to over 100 m, depending on the electrode spacing. The distance between electrodes determines the detection depth and affects the desired resolution. In both the Schlumberger-Wenner and gradient arrays, the maximum detection depth is estimated to be approximately one-fifth of the maximum separation between the current electrodes C1 and C2, as shown in Figure 5. When designing measurements, it is important to remember that increasing the distance between electrodes enhances depth range detection at the expense of resolution. Consequently, layers with minimal thickness may become undetectable, and the recorded resistivity value represents the average resistivity across all thin layers. Complete depth detection is typically confined to the central parts of the profile. The edge zones of the resistivity cross-section are most prone to significant RMS (root mean square) error, a consequence of the research methodology and the inversion of measurement data, as detailed in the User's Manual for Res2D and 3D (2001).

SCOPE OF FIELDWORK

Measurements were made using a symmetrical Schlumberger-Wenner array along two profiles approximately perpendicular to each other: profile A–B with a W–E orientation and profile C–D with an N–E orientation. The unit distance between electrodes for A–B and C–D was set at 2.5 m, resulting in a mainline length of 100 m. With two repositions of the measuring cable, 50 m each, the final length of the profiles was extended to 200 m. The profiles intersected at a shallow geological borehole, 9 m deep. Additionally, along the trace of the AB profile, measurements were conducted with a doubled unit spacing between electrodes, set at 5 m, resulting in a mainline length of 200 m for profile A'–B'. Each repositioning of the measuring cable did not alter the depth of detection afforded by the length of the main sequence but increased the length of full detection along the designed profile (Fig. 5). The XYZ coordinates for each electrode were determined using GPS. Given the area's topography, all results were interpreted using *Res2D* software. The inversion was done using the modify smoothness algorithm – constrained least-squares method, taking into account the topography, maximum iteration quantity was 5. The locations of the measurement profiles are shown in Figure 1C.

RESULTS OF ELECTRICAL RESISTIVITY TOMOGRAPHY

The obtained resistivity cross-sections reveal a distinctly layered structure with relatively low resistivity values, ranging from 15 to 235 m (Fig. 6). The depth of detection along the A–B and C–D profiles is ~20m, while for the A'–B' profile, it is ~40 m, due to the applied unit spacing of the electrodes. All cross-sections are characterised by very low RMS error values, indicating an excellent fit of the obtained models to the studied geological medium and, consequently, their high credibility.

In the resistivity image, starting from the top, there are four layers in sections A–B and C–D, and five layers in section A'–B'. Layer no. 1, with a resistivity of ~50–100 m, maintains a consistent thickness of ~1.5–2 m. Layer no. 2, showing a resistivity of 20–50 m, has a thickness of around 10 m and is consistently stable. Its apparent increase is observed at the beginning of the A–B profile and the end of the C–D profile, also confirmed in the deeper A'–B' profile. Beneath layer no. 2 is a thin layer no. 3, ~2.5 m thick, with a resistivity of ~50–110 m. On the A–B and A'–B' profiles, a collapse of this layer is observed, similar to layer no. 2, from ~40 m towards their start and on the C–D profile from ~150 m towards its end. The next layer, no. 4, has a resistivity ranging from ~120–300 m. Its total thickness, visible only in the deeper A'–B' section, reaches ~25 m. The base of this layer was not reached on the A–B and C–D profiles. Its ceiling is undulating with noticeable depressions, visible only in shallow cross-sections. The deeper resistivity cross-section A'–B' revealed another low-resistivity layer - layer no. 5. Its top is identified at a depth of ~35 m, with a resistivity range similar to layer no. 2 (20–50 m). In the deep cross-section A'–B', the layer boundaries are smoother, while in the shallower A–B and C–D cross-sections, the edges are more sharply defined.

INTERPRETATION OF ELECTRICAL RESISTIVITY CROSS-SECTIONS

The electrical resistivity cross-sections obtained (Fig. 6) are characterised by very low RMS error values (1.0–1.3%), indicating a perfect fit of the measurement data to the interpreted theoretical model and confirming an ideal match with the geological conditions. In the cross-sections, the uppermost layer, layer no. 1, is visible only in Figure 6A and C and is associated with the present-day soil. Layer no. 2, also visible in these figures, correlates well with the loess L1 identified in the study area, confirming the results of shallow geological drilling to a depth of 9 m (Łanczont et al., 2014). The slightly higher electrical resistivity values in the ceiling of the loess cover, reaching ~90 m, can be associated with lower moisture content and a small amount of sand.

Directly under the loess cover is a thin layer of fossil palaeosol S1 – layer no. 3 (Fig. 6A, C), also evident in the borehole. This soil has a granulometric composition different from the loess (Fig. 3A, B), making it a slightly worse conductor. The relatively wide range of electrical resistivity in this layer may result from the presence of loess material, with mixing of loess and soil material or the presence of thin loess

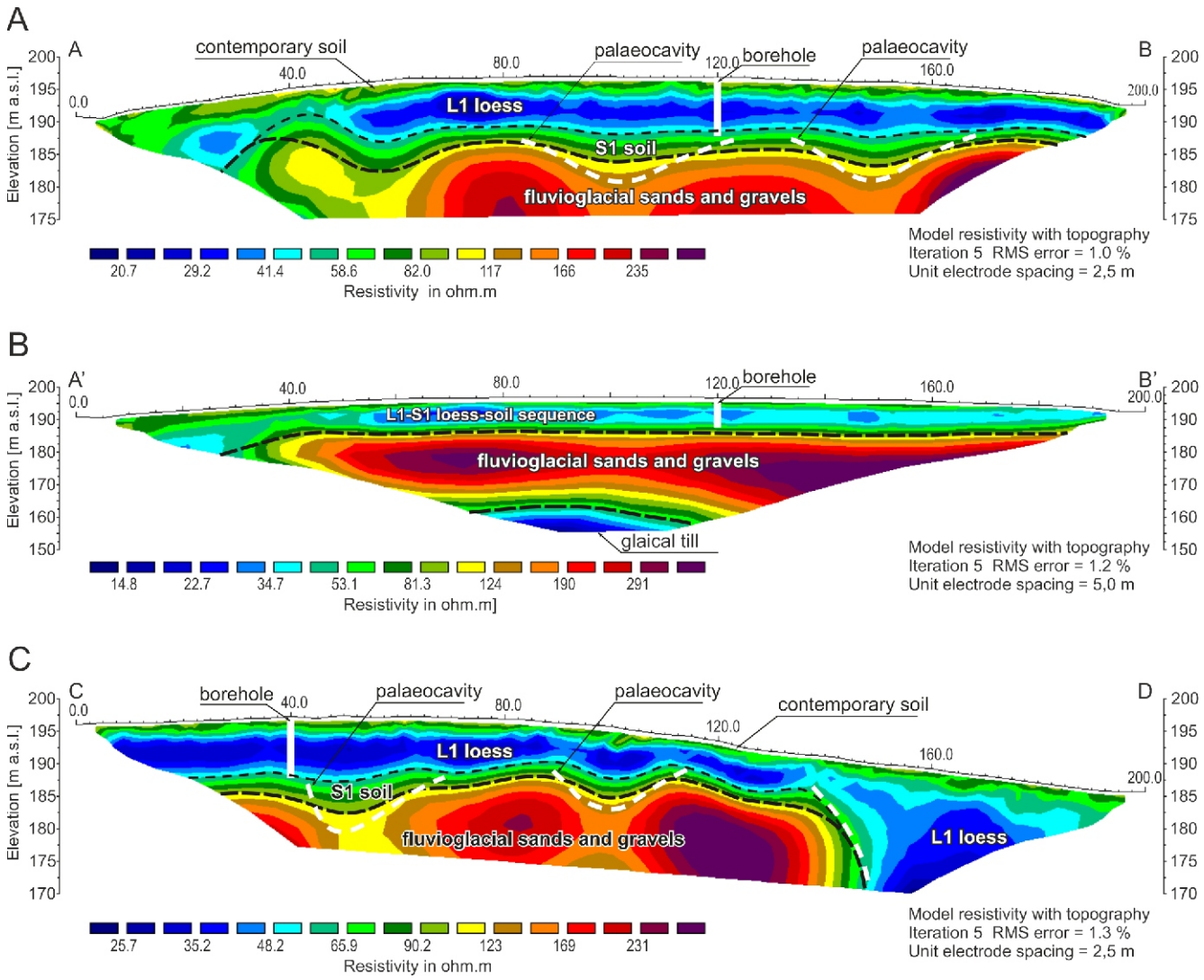

Fig. 6. Electrical resistivity of three cross-sections located in the vicinity of the archaeological site Wilczyce 10

The paths of these cross-sectional lines are indicated in Figure 1C

laminae causing visible changes in resistivity value. However, the resolution of the research prevents isolation of individual several-centimetre laminae.

The three formations described in Figure 6B form one large sedimentary complex known as the L1-S1 loess-palaeosol sequence. The lack of detailed recognition of sediments in this area is due to the lower resolution, a result of the electrodes being twice the distance apart compared to the main sequence on the A–B and C–D profiles. As the distance between the electrodes increases, the recognition depth increases and the resolution decreases. In the bedrock of layer no. 3, there is a complex of fluvioglacial sand and gravel sediments – layer no. 4 (Fig. 6), characterised by a relatively low range of electrical resistivity, possibly due to moisture or water containment. The morphology of their ceiling is accurately reflected in the high-resolution shallow profiles A–B and C–D (Fig. 6A, C), which show an irregular surface with two distinct palaeo-cavities covered with S1 fossil soil and L1 loess. The greater exploration depth of the deep profile A'–B' (Fig. 6B) allowed for determining the depth of their bottom and estimating their thickness at ~25 m. However, the greater depth results in lower resolution, as seen in the smoother morphology of the ceiling in this profile.

Finally, the deep electrical resistivity cross-section A'–B' (Fig. 6B) identified another layer – layer no. 5, characterised by the same resistivity values as the loess L1 layer (20–50 m) and associated with the presence of glacial till.

When comparing the three described cross-sections, despite similar resistivity ranges, noticeable differences are evident. High resolution was achieved with a short main profile (100 m) in the A–B and C–D profiles (Fig. 6A, B). This allowed for the precise recognition of thin, shallow layers and the accurate determination of their boundaries. However, the depth of recognition is limited, at ~20 m. With a longer main profile (200 m) – as in profile A'–B' (Fig. 6B) – the number of measurement points per unit of length is half that of the shallow A–B and C–D profiles. Consequently, the resolution is lower, but the recognition depth is greater, around 40 m. Due to this lower resolution, the boundaries of the layers appear smoothed and lie horizontally. The shallow layers (layers no. 1–3) were identified as a single loess-soil sequence. Meanwhile, the greater exploration depth not only allowed for determining the lower part of the fluvioglacial sands and gravels (layer 4) but also for identifying the presence of layer 5 – glacial till.

DISCUSSION WITH GEOMORPHOLOGICAL APPLICABILITY

Electrical resistivity cross-section conducted along two straight lines perpendicular to each other (Fig. 6) revealed the continuity of the youngest loess layer (L1), which is commonly recognised as a typical feature of loess from the last cycle of aeolian sedimentation in Europe (e.g., Frechen, 2003; Smalley, 2011; Rousseau, et al., 2018; Lehmkuhl et al., 2021). However, the cross-section showed variable thickness of these covers, ranging from ~5 to a maximum of 15 m. This is consistent with the recognition of loess covers in the Sandomierz-Opatów region conducted, among others, by Lindner (1972), Jersak et al. (1992) and Czarnecki (2005). These thicknesses are also typical for periglacial loess of the Weichselian age in Europe and fall within the average values between the "oceanic" thin loesses of the western part of the continent and the several-metre or over 20 m thickness documented in the continental east (e.g., Łanczont et al., 2022). The thickness of the L1 loess here is similar to that of loesses of this age described in the nearby, key-site of Złota (also known as Polanów Samborzecki; e.g., Dolecki and Łanczont, 1998; Jary, 2007; Mroczek, 2013; Moska et al., 2015; Skurzyński et al., 2024). These sites differ geomorphologically: Wilczyce is situated on a loess plateau, whereas Złota lies at the edge of a loess patch, adjacent to the Vistula River Valley. Despite similarities in luminescence age (TL, OSL) and litho-pedological formations in both profiles, Wilczyce features much finer mean grain size (median) and better-sorted sediments. This suggests selective wind-blown particle transport from their primary source at the bottom of the Vistula River Valley. In Złota, the sediment results from very short-distance transport, whereas in Wilczyce, the source is several kilometres away (Pańczyk et al., 2020).

Presented in Figure 6, the differing resistivity characteristics of the loess and the underlying layers allow for the unambiguous lithological identification of the sediments. Based on the resistivity image, it can be concluded that the L1 loess forms a continuous layer completely covering the older, genetically different substrate. The varying resistivity recorded in different parts of the electrical resistivity profiles indicates that the loess was accumulated on a surface with significant, several-metre-level elevations. The intra-loess palaeo-surface has a wavy course, which in a spatial context likely corresponds to concave linear forms (small valleys) and/or closed depressions separated by convex watersheds. Moreover, a very steep fossil edge of the buried layer, ~10 m high (Fig. 6C), was completely buried as a result of aeolian accumulation of L1 loess, reaching a thickness of at least 15 m here. This is an example of landscape inversion that occurred due to the dense covering (masking) of older landforms under a loess mantle. Similar masking of the older substrate under Weichselian loess identified in electrical resistivity profiles was also demonstrated by Żogała (2015) in the Upper Dnister region and the Podillia Upland (Western Ukraine) and Kołodyńska-Gawrysiak (2019) in the westernmost part of Wolhynian region (Eastern Poland).

The identification of the S1 palaeosol complex in the lower decimetres of the drill core (Figs. 4 and 5) allows for the interpretation of layers from the electrical resistivity image. The wavy palaeo-surface described above should also be identified with soil horizons formed at the top of fluvioglacial deposits. In Figure 6, this is evident in the diffusive change in resistivity. Additionally, these changes suggest that there are various morphologies of soil profiles, and perhaps also a varying degree of preservation of the S1 soil complex. In neighboring exposures (e.g., Złota, referenced literature above), the soil complex is documented as interglacial, either fully or partially eroded Luvisol with superimposed interstadial chernozem horizons, corresponding together to the evolution of a relatively warm MIS5 environment and their subsequent periglacial transformation in MIS 4.

The leveled top of the loess cover at the Wilczyce 10 site is characterized by various soil types, as documented during fieldwork (Łanczont et al., 2014, 2015b). The diverse morphology of soil profiles suggests active soil erosion processes and concurrent leveling of the topographic surface. The varying degrees of development in profiles at the top of the loess (Fig. 1C) imply significant undulations in the original relief, likely indicative of a wavy landscape formed in a periglacial environment during the final stage of the aeolian deposition period. This type of aeolian character of the loess landscape was reconstructed by Rodzik et al. (2014) based on studies of the soil cover at the Magdalenian site in Klementowice (the Nałęczów Plateau), located just ~70 km to the NE of Wilczyce. Similar geomorphological conclusions related to the transformation of Luvisols into Regosols developed on loess were reached by Loba et al. (2023), based on examples from SW Poland. However, in the case of Wilczyce, this variability in soil cover formation was documented indirectly through geophysical methods along two straight-line profiles in a catena arrangement, as well as toposequences.

Electrical resistivity cross-section confirmed the recognition of lithologically differentiated layers documented in the drill core by Łanczont et al. (2014, 2015b), as well as earlier by Bielecka (1968a, b). Similarly, interglacial soils (S1, S0) were well recognised, while mid-loess palaeosols of lower stratigraphic rank were poorly identified. This primarily concerns the interstadial MIS 3 soil – described in the drill core (Figs. 2 and 3), and also available in the exposure at Złota (referenced literature above). In the electrical resistivity images, there is also a lack of recognition of lower stratigraphic rank soils identified within the loess L1LL1, which are fundamentally poorly developed (gleysol horizons) and have a thickness of only a few decimeters. The presence of such 1–3 palaeosols in the loess of the Upper Pleniglacial has been found in many central European profiles (e.g., Maruszczak, 1991, 1995; Jary, 2004; Antoine et al., 2009, 2013; Fedorowicz et al., 2013).

CONCLUSIONS

Geophysical surveys of the loess cover have demonstrated the effectiveness of this method in studying the characteristics of loess covers – particularly in analysing their litho- and pedological formation, as well as determining their relationship to the bedrock. The conducted research enables a number of conclusions to be drawn, related to both electrical resistivity tomography and the geomorphological nature:

- the ERT method in this study enabled complete rock mass recognition to a depth determined by the main profile length;
- in the 100 m profile, high resolution allowed precise recognition up to ~20 m, distinguishing four geological layers: modern soil, loess L1, and fossil soil S1 correlated with data from a shallow 9 m borehole; layer 4 comprised fluvioglacial sands and gravels below exploration depth;
- in the 200 m profile, recognition extended to around 40 m, with lower resolution identifying three thicker geological layers: L1-S1 loess-palaeosol sequence (contemporary soil, L1 loess, S1 fossil soil), fluvioglacial sands and gravels, and low-resistivity glacial till (base below recognition depth);

– high-resolution sequences precisely delineated layer boundaries, revealing distinct palaeorelief on top of fluvioglacial sands and gravels, along with large palaeocavities beneath fossil palaeosol S1 and loess L1 deposits, facilitating older relief reconstruction.

The studies presented above also allow us to draw a number of conclusions about the characteristics of the L1 loess cover – the most important of which are:

– the ERT method confirms L1 loess continuity, a key feature of recent aeolian sedimentation in Europe, with variable thickness (5–15 m), typical for Weichselian periglacial loess;
– clear lithological identification via electrical resistivity imaging reveals a wavy palaeo-surface under the loess layer, indicating undulations in the original relief, crucial for understanding geomorphological evolution and soil transformations under the loess mantle;
– the typological diversity of soils at the top of the loess cover indicates intense erosion and leveling of the original landforms. The interglacial paleosol (S1) is clearly identified, but palaeosols of lower stratigraphic rank are poorly documented. This points to the complexity of the soil formation processes and the challenges in detecting underdeveloped horizons using electrical resistivity cross-sections.

Acknowledgements. We dedicate this publication to Prof. Dr. hab. Romuald Schild (1936–2021), who invited and inspired our team to carry out research on the identification of the palaeoenvironment in the vicinity of the Late Magdalenian site in Wilczyce. We thank two anonymous reviewers for their helpful comments. We would like to extend sincere thanks to editors – W. Granoszewski and J. Rotnicka – for their constructive comments and supervision of this paper.

REFERENCES

Antoine, P., Rousseau, D.-D., Moine, O., Kunesch, S., Hatté, C., Lang, A., Zöller, L., 2009. Evidence of rapid and cyclic eolian deposition during the Last Glacial in European loess series (loess events): The high-resolution records from Nussloch (Germany). Quaternary Science Reviews, **28**: 2955–2973; https://doi.org/10.1016/j.quascirev.2009.08.001

Antoine, P., Rousseau, D.-D., Degeai, J.-P., Moine, O., Lagroix, F., Kreutzer, S., Fuchs, M., Hatté, Ch., Gauthier, C., Svoboda, J., Lisá, L., 2013. High-resolution record of the environmental response to climatic variations during the Last Interglacial–Glacial cycle in Central Europe: the loess–palaeosol sequence of Dolní Věstonice (Czech Republic). Quaternary Science Reviews, **67**: 17–38; https://doi.org/10.1016/j.quascirev.2013.01.014

Bałaga, K., Hołub, B., Komar, M., Kusiak, J., Łanczont, M., Mroczek, P., Zieliński, P., 2008. Próba rekonstrukcji rzeźby terenu i środowiska z okresu funkcjonowania późnomagdaleńskiego obozowiska w Wilczycach (Wyżyna Sandomierska) (in Polish). Landform Analysis, **9**: 269–271.

de Bari, C., Lapenna, V., Perrone, A., Puglisi, C., Sdao, F., 2011. Digital photogrammetric analysis and electrical resistivity tomography for investigating the Picerno landslide (Basilicata region, southern Italy). Geomorphology, **133**: 34–46; https://doi.org/10.1016/j.geomorph.2011.06.013

Deeben, J., Hiddink, H., Huisman, D.J., Müller, A., Schokker, J., Wallinga, J., 2010. Middle Palaeolithic artefact migration due to periglacial processes; a geological investigation into near-surface occurrence of Palaeolithic artefacts (Limburg-Eastern Brabant coversand region, the Netherlands). Netherlands Journal of Geosciences, Geologie en Mijnbouw, **89**: 35–50; https://doi.org/10.1017/S0016774600000809

Bian, S., Chen, G., Zeng, R., Meng, X., Jin, J., Lin, L., Zhang, Y., Shi, W., 2022. Post-failure evolution analysis of an irrigation-induced loess landslide using multiple remote sensing approaches integrated with time-lapse ERT imaging: lessons from Heifangtai, China. Landslide, **19**: 1179–1197; https://doi.org/10.1007/s10346-022-01859-x

Bielecka, M., 1968a. Detailed Geological Map of Poland 1:50,000, sheet Sandomierz (in Polish). Wyd. Geol., Warszawa.

Bielecka, M., 1968b. Explanations to the Detailed Geological Map of Poland 1:50,000, sheet Sandomierz (in Polish). Wyd. Geol., Warszawa.

Chlebowski, R., Lindner, L., 1991. Sources of material and conditions of the younger loesses accumulation in the Małopolska Upland (in Polish with English summary). Biuletyn Geologiczny, **32**: 15–50.

Czarnecki, R., 2005. Wyżyna Sandomierska. Część Wschodnia. II. Struktura krajobrazu geograficznego (in Polish). Warszawa.

Dolecki, L., Łanczont, M., 1998. Loesses and paleosols of the older part of the Wisła (Würm) glaciation in Poland. Geologija, **25**: 31–38.

Fabregat, I., Gutiérrez, F., Roqué, C., Comas, X., Zarroca, M., Carbonel, D., Guerrero, J., Linares, R., 2017. Reconstructing the internal structure and long-term evolution of hazardous sinkholes combining trenching, electrical resistivity imaging (ERI) and ground penetrating radar (GPR). Geomorphology, **285**: 287–304; https://doi.org/10.1016/j.geomorph.2017.02.024

Fedorowicz, S., Łanczont, M., Bogucki, A., Kusiak, J., Mroczek, P., Adamiec, G., Bluszcz, A., Moska, P., Tracz, M., 2013. Loess–paleosol sequence at Korshiv (Ukraine) – chronology based on complementary and parallel dating (TL, OSL), and litho–pedosedimentary analyses. Quaternary International, **296**: 117–130; https://doi.org/10.1016/j.quaint.2012.06.001

Feng, L., Lin, H., Zhang, M., Guo, L., Jin, Z., Liu, X., 2020. Development and evolution of loess vertical joints on the Chinese Loess Plateau at different spatiotemporal scales. Engineering Geology, **265**; https://doi.org/10.1016/j.enggeo.2019.105372

Fiedorczuk, J., Schild, R., 2002. Wilczyce – a new late Magdalenian site in Poland. In: Recent Studies in the Final Palaeolithic of the European Plain (eds. B.V. Eriksen and B. Bratlund): 91–100. Jutland Archaeological Society, Gylling.

Folk, L.R., Ward, W.C., 1957. Brazos River bar: a study in the significance of grain size parameters. Journal of Sedimentary Petrology, **27**: 3–26; https://doi.org/10.1306/74D70646-2B21-11D7-8648000102C1865D

Frankowski, Z., Grabowski, D., 2006. Engineering-geological and geomorphological conditions of gully erosion in loess deposits in the Kazimierz Dolny area (Opolska Droga Gully) (in Polish with English summary). Przegląd Geologiczny, **54**: 777–783.

Frechen, M., 2003. Loess in Europe—mass accumulation rates during the Last Glacial Period. Quaternary Science Review, **22**: 1835–1857; https://doi.org/10.1016/S0277-3791(03)00183-5

Gilewska, S., 1972. Wyżyny Śląsko-Małopolskie (in Polish). In: Geomorfologia Polski (ed. M. Klimaszewski), **1**: 232–339. Polska Południowa, Góry i Wyżyny. PWN Warszawa.

Haase, D., Fink, J., Haase, G., Ruske, R., Pécsi, M., Richter, H., Altermann, M., Jäger, K.-D., 2007. Loess in Europe—its spatial distribution based on a European Loess Map, scale 1:2,500,000. Quaternary Science Reviews, **26**: 1301–1312; https://doi.org/10.1016/j.quascirev.2007.02.003

Instrukcja obsługi programu Res2Dinv, 2011. Geoelectrical Imaging 2D and 3D. Geotomo Software.

Jary, Z., 2007. Record of Climate Changes in Upper Pleistocene loess-soil sequences in Poland and western part of Ukraine (in Polish with English summary). Rozprawy Naukowe Instytutu Geografii Rozwoju regionalnego Uniwersytetu Wrocławskiego, Wrocław.

Knödel, K., Lange, G., Voigt, H.-J., 2007. Environmental Geology. Handbook of Field Methods and Case Studies. Springer, Berlin.

Kołodyńska-Gawrysiak, R., 2019. The impact of palaeorelief on the origin of same closed depressions in loess areas in the Lublin Upland (Eastern Poland). Polish Journal of Soil Science, **52**: 1–12; https://doi.org/10.17951/pjss.2019.52.1.1

Kolstrup, E., Schild, R., 2014. The Wilczyce ice wedge cast system. Testimony of Weichselian permafrost in Southern Poland and preserver of artifacts and fauna. In: A Late Magdalenian Winter Hunting Camp in Southerm Poland (ed. R. Schild): 81–86. Institute of Archaeology and Ethnology Polish Academy of Sciences. Warszawa.

Kowalska, J.B., Vögtli, M., Kierczak, J., Egli, M., Waroszewski, J., 2022. Clay mineralogy fingerprinting of loess-mantled soils on different underlying substrates in the south-western Poland. Catena, **210**, 105874; https://doi.org/10.1016/j.catena.2021.105874

Kukla, G., An, S., 1989. Loess stratigraphy in central China. Palaeogeography, Palaeoclimatology, Palaeoecology, **72**, 203–225; https://doi.org/10.1016/0031-0182(89)90143-0

Lehmkuhl, F., Nett, J.J., Pötter, S., Schulte, P., Sprafke, T., Jary, Z., Antoine, P., Wacha, L., Wolf, D., Zerboni, A., Hošek, J., Marković, S.B., Obreht, I., Sümegi, P., Veres, D., Zeeden, C., Boemke, B.J., Schaubert, V., Viehweger, J., Hambach, U., 2021. Loess landscapes of Europe – mapping, geomorphology, and zonal differentiation. Earth-Science Reviews, **215**: 103496; https://doi.org/10.1016/j.earscirev.2020.103496

Li, Y., Shi, W., Aydin, A., Beroya-Eitner, M.A., Gao, G., 2020. Loess genesis and worldwide distribution. Earth-Science Reviews, **201**: 102947; https://doi.org/10.1016/j.earscirev.2019.102947

Lindner, L., 1976. Conditions of younger loess accumulation in the western part of the Świętokrzyskie region (in Polish with English summary). Biuletyn Instytutu Geologicznego, **297**: 307–312.

Ling, C., Xu, Q., Zhang, Q., Ran, J., Lv, H., 2016. Application of electrical resistivity tomography for investigating the internal structure of a translational landslide and characterising its groundwater circulation (Kualiangzi landslide, Southwest China). Journal of Applied Geophysics, **131**: 154–162; https://doi.org/10.1016/j.jappgeo.2016.06.003

Loba, A., Zhang, J., Tsukamoto, S., Kasprzak, M., Kowalska, J.B., Frechen, M., Waroszewski, J., 2023. Multiproxy approach to the reconstruction of soil denudation events and the disappearance of Luvisols in the loess landscape of south-western Poland. Catena, **220**: 106724; https://doi.org/10.1016/j.catena2022.106724

Loke, M.H., 1999. Electrical imaging surveys for environmental and engineering studies. Available at web address: www.geometrics.com

Loke, M.H., 2011. Electrical Resistivity Surveys and Data Interpretation. In: Encyclopedia of Solid Earth Geophysics (ed. H.K. Gupta). Encyclopedia of Earth Sciences Series. Springer, Dordrecht; https://doi.org/10.1007/978-90-481-8702-7_46

Łanczont, M., Wilgat, M., 1994. Differentiation of the Carpathian Loess in Przemyśl environs in the light of heavy minerals analysis (in Polish with English summary). Annales UMCS, sec. B, **49:** 81–99.

Łanczont, M., Mroczek, P., Zieliński, P., Hołub, B., Kusiak, J., Bałaga, K., Komar, M., Łącka, B., Żogała, B., Mendecki, M., 2014. Regional Paleogeographic Analysis of Site Wilczyce 10 in the Opatówka Valley and the Stratigraphic Context of the Wedge Cast. In: A Late Magdalenian Winter Hunting Camp in Southerm Poland (ed. R. Schild): 31–80. Institute of Archaeology and Ethnology Polish Academy of Sciences, Warszawa.

Łanczont, M., Bogucki, A., Mroczek, P., Hołub, B., Żogała, B., Fedorowicz, S., Kusiak, J., 2015a. The influence of local relief on the variability of loess accumulation conditions – case study: Halych site on the Dniester River (Eastern Carpathian Foreland, Ukraine). Proc. International Symposium on Aeolian Deposits in Earth History. Beijing, China.

Łanczont, M., Madeyska, T., Mroczek, P., Hołub, B., Żogała, B., Bogucki, A., 2015b. Relief and palaeorelief analyses of the Kraków Spadzista Palaeolithic site as the tools used for explanation of the site location. Quaternary International, **359–360**: 89–95; https://doi.org/10.1016/j.quaint.2014.03.045

Łanczont, M., Mroczek, P., Madeyska, T., Komar, M., Hołub, B., Żogała, B., Sobczyk, K., Wilczyński, J., 2015c. Natural environment of the Gravettian settlement in the Kraków Spadzista site based on palaeogeographical interpretation of loess-palaeosol sequences. In: A Gravettian Site in Southern Poland: Kraków Spadzista (eds. G. Haynes, P. Wojtal and J. Wilczyński): 19–49. ISEA PAS, Kraków.

Łanczont, M., Mroczek, P., Komar, M., Fedorowicz, S., Woronko, B., Nawrocki, J., Frankowski, Z., Standzikowski, K., 2022. A remarkable last glacial loess sedimentation at Roxolany in the Dniester Liman (Southern Ukraine). Quaternary Science Review, **285**: 107521; https://doi.org/10.1016/j.quascirev.2022.107521

Makowski, J., 1976. Causes of variation in the density of the gully network in the Kielce-Sandomierz Upland (in Polish with English summary). Prace i Studia Instytutu Geografii UW, **21**: 49–75.

Malinowski, J., 1959. Results of geotechnical investigations on loess between Kazimierz Dolny and Nałęczów (in Polish with English summary). Kwartalnik Geologiczny, **3** (4): 425–456.

Malinowski, J., 1971. Badania geologiczno-inżynierskie lessów (in Polish). Wyd. Geol., Warszawa.

Marković, S., Bokhorst, M., Vanderberghe, J., McCoy, W., Oches, E., Hambach, U., 2008. Late Pleistocene loess-paleosol sequences in the Vojvodina region, north Serbia. Journal of Quaternary Science, **23**: 73–84; https://doi.org/10.1002/jqs.1124

Marković, S., Stevens, T., Kukla, G.J., Hambach, U., Fitzsimmons, K.E., Gibbard, P., Buggle, B., Zech, M., Guo, Z., Hao,Q., Wu, H., O'Hara Dhand, K., Smalley, I.J., Újvári, G., Sümegi, P., Timar-Gabor, A., Veres, D., Sirocko, F., Vasiljević, D.A., Jary, Z., Svensson, A., Jović, V., Lehmkuhl, F., Kovács, J., Svirčev, Z., 2015. Danube loess stratigraphy – towards a pan-European loess stratigraphic model. Quaternary Science Reviews, **148**: 228–258; https://doi.org/10.1016/j.earscirev.2015.06.005

Maruszczak, H., 1991. Stratigraphic differentiation of Polish loesses (in Polish with English summary). In: Podstawowe profile lessów w Polsce, Lublin (ed. H. Maruszczak): A.13–A.15.

Maruszczak, H., 1995. Glacial cycles of loess accumulation in Poland during the last 400 ka and global rythms of paleogeographical events. Annales UMCS, sec. B, **50**: 127–156.

Maruszczak, H. (ed.), 2001. Main sections of loess in Poland II (in Polish with English summary). Wydawnictwo UMCS, Lublin.

Maruszczak, H., Wilgat, M., 1995. Stratigraphical and paleogeographical interpretation of the results of heavy minerals analysis in loess of Voivodina. Annales UMCS, B, **50**: 173–190.

Mendecki, M., Zuberek, W., Żogała, B., 2013. Determination of the extent of fractured zones around the mine openings sing the resistivity and GPR methods. Rock Mechanics for Resources, Energy and Environment: proceeding of EUROCK ISRM International Symposium, Wrocław.

Moska, P., Jary, Z., Adamiec, G., Bluszcz, A., 2015. OSL chronostratigraphy of a loess-palaeosol sequence in Złota using quartz and polymineral fine grains. Radiation Measurements. **81**: 23–31; https://doi.org/10.1016/j.radmeas.2015.04.012

Mroczek, P., 2013. Recycled loesses - A micromorphological approach to the determination of local source areas of Weichselian loess. Quaternary International, **296**: 241–250; https://doi.org/10.1016/j.quaint.2013.02.040

Mroczek, P., 2018. Late Vistulian-Holocene evolution of loess soils of the southern Polish uplands in the light of micromorphological studies (in Polish with English summary). Wydawnictwo UMCS, Lublin.

Pańczyk, M., Nawrocki, J., Bogucki, A.B., Gozhik, P., Łanczont, M., 2020. Main features of the age spectra of detrital zircons from loess deposited in Poland and Ukraine: possible sources of detritus and pathways of its supply. Aeolian Research **45**: 100598; https://doi.org/10.1016/j.aeolia.2020.100598

Plewa, M., Plewa, S., 1992. Petrofizyka (in Polish). Wyd. Geol., Warszawa.

Qin, P., Liu, Y., Song, Z., Ma, F., Wang, Y., Zhang, X., Miao, Ch., Dong, X., 2020. An electrical resistivity method of characterizing hydromechanical and structural properties of compacted loess during constant rate of strain compression. MDPI Sensors, **20**: 4783; https://doi.org/10.1016/j.aeolia.2020.100598

Racinowski, R., 1976. Remarks on the heavy minerals composition of the Lublin and Przemyśl loesses (in Polish with English summary). Biuletyn Instytutu Geologicznego, **297**: 227–246.

Rodzik, J., Mroczek, P., Wiśniewski, T., 2014. Pedological analysis as a key for reconstructing primary loess relief – a case study from the Magdalenian site in Klementowice (eastern Poland). Catena, **117**: 50–59; https://doi.org/10.1016/j.catena.2013.09.001

Rousseau, D.-D., Derbyshire, E., Antoine, P., Hatté, C., 2018. European Loess Records. In: Reference Module in Earth Systems and Environmental Sciences. Elsevier; https://doi.org/10.1016/B978-0-12-409548-9.11136-4

Ryncarz, T., 1993. Zarys fizyki górotworu (in Polish). Śląskie Wydawnictwo Techniczne, Katowice.

Samsonowicz, J., 1960. The Lower Cambrian of the Klimontów antyklinorium. International Geological Congres XXI, Report of the Session Norden, Pt. VIII, Late Pre-Cambrian and Cambrian Stratigraphy, Copenhagen: 88–92.

Schön, J.H., 1996. Physical Properties of Rocks: Fundamentals and Principles of Petrophysics. Pergamon – Elsevier Science Inc. New York.

Skurzyński, J., 2020. Chemostratigraphy and spatial variability of the chemical composition of the Late Pleistocene loess-palaeosol sequences in Poland (in Polish). Ph.D. thesis, Archive of University of Wrocław.

Skurzyński, J., Jary, Z., Raczyk, J., Moska, P., Korabiewski, B., Ryzner, K., Krawczyk, M., 2019. Geochemical characterisation of the Late Pleistocene loess-palaeosol sequence in Tyszowce (Sokal Plateau-Ridge, SE Poland). Quaternary International, **502**, 108–118; https://doi.org/10.1016/j.quaint.2018.04.023

Skurzyński, J., Jary, Z., Fenn, K., Lehmkuhl, F., Raczyk, J., Stevens, T., Wieczorek, M,. 2024. Implications of the geochemistry of L1LL1 (MIS2) loess in Poland for paleoenvironment and new normalizing values for loess-focused multi-elemental analyses. Quaternary Research, First View: 1–18; https://doi.org/10.1017/qua.2023.69

Smalley, I., Marković, S.B., Svirčev, Z., 2011. Loess is [almost totally formed by] the accumulation of dust. Quaternary International, **240**: 4–11; https://doi.org/10.1016/j.quaint.2010.07.011

Stenzel, P., Szymanko, J., 1973. Metody geofizyczne w badaniach hydrogeologicznych i geologiczno-inżynierskich (in Polish). Wyd. Geol., Warszawa.

Tomczyk, H., 1974. Góry Świętokrzyskie (in Polish). In: Budowa Geologiczna Polski. Tektonika, **4**: 128–197. Wyd. Geol., Warszawa**.**

User manual Geoelectrocal Imaging 2D& 3D Geotomo Software, 2001.

Ward, S.H., 1990. Resistivity and induced polarisation methods. In: Geotechnical and Environmental Geophysics – Investigations in Geophysics (ed. S. Ward), **5**: 169–189. Society of Exploration Geophysicists, Tulsu OK/USA, SEG.

Whiteley, J.S., Chambers, J.E., Uhlemann, S., Wilkinson, P.B., Kendall, J.M., 2019. Geophysical monitoring of moisture-induced landslides: a review. Reviews of Geophysics, **57**: 106–145; https://doi.org/10.1029/2018RG000603

Zeng, R.Q., Meng, X.M., Zhang, F.Y., Wang, S.Y., Cui, Z.J., Zhang, M.S., Zhang. Y., Chen. G., 2016. Characterising hydrological processes on loess slopes using electrical resistivity tomography – A case study of the Heifangtai Terrace, Northwest China. Journal of Hydrology, **541**: 742–753; https://doi.org/10.1016/j.jhydrol.2016.07.033

Zhang, B., Feng, L., Zhang, M., Sun, P., Li, T., Liu, H., 2022. Application of resistivity measurement to stability evaluation for loess slopes. Landslides, **19**: 2871–2887; https://doi.org/10.1007/s10346-022-01951-2

Zhao, K., Xu, Q., Liu, F., Xiu, D., Ren, X., 2020. Field monitoring of preferential infiltration in loess using time-lapse electrical resistivity tomography. Journal of Hydrology, **591**; https://doi.org/10.1016/j.jhydrol.2020.125278

Żogała, B., 2013. Geoelectrical methods in the research of soils contaminated with petroleum products (in Polish with English summary). Wydawnictwo Uniwersytetu Śląskiego, Katowice.

Żogała, B., Stan-Kłeczek, I., 2022. Wykorzystanie tomografii elektrooporowej do rozpoznania pokryw lessowych (in Polish). In: Metodyka rekonstrukcji zmian klimatu i środowiska zapisanych w pokrywach lessowych (eds. M. Łanczont, B. Hołub and P. Mroczek): 89-94. XXI Terenowe Seminarium Korelacja lessów i osadów glacjalnych Polski i Ukrainy. Interdyscyplinarne Seminarium Naukowe Glacjał i peryglacjał Europy Środkowej. Jarosław, 6–8 października 2022 r., Lublin.

Żogała, B., Łanczont, M., Hołub, B., Bogucki, A., Mroczek, P., 2015. Rozpoznanie elektrooporowe wybranych paleolitycznych stanowisk lessowych strefy pery- i metakarpackiej (in Polish). In: Paleolityczna ekumena strefy pery- i metakarpackiej (eds. M. Łanczont and T. Madeyska): 459–485. Wydawnictwo Uniwersytetu Marii Curie-Skłodowskiej, Lublin.